




# Multiscale modeling of the shock-induced chemical reaction in Al/Ni composites

Wei Xiong<sup>1,2</sup>, Xianfeng Zhang<sup>1,\*</sup> , Haihua Chen<sup>3</sup>, Mengting Tan<sup>1</sup>, and Chuang Liu<sup>1</sup>

<sup>1</sup>School of Mechanical Engineering, Nanjing University Science and Technology, Xiaolingwei 200, Nanjing 210094, China

<sup>2</sup>State Key Laboratory of Explosion Science and Technology, Beijing Institute of Technology, Beijing 100081, China

<sup>3</sup>Shanghai Electro-Mechanical Engineering Institute, Shanghai 201109, China

**Received:** 5 August 2022

**Accepted:** 31 October 2022

**Published online:**

8 November 2022

© The Author(s), under exclusive licence to Springer Science+Business Media, LLC, part of Springer Nature 2022

## ABSTRACT

A multiscale modeling method was proposed to describe the shock-induced chemical reaction (SICR) in Al/Ni composites, especially with large particle sizes of hundreds of micrometers. A one-dimension reaction diffusion model was established firstly based on the Fick's second law, by which the reaction and mass diffusion process between single Al and Ni particle were calculated. Two critical parameters in the reaction–diffusion model were determined. Furthermore, mesoscale simulation on SICR of Al/Ni composites was proposed. A subroutine to describe the SICR process was created based on Mie–Grüneisen equation of state and the reaction–diffusion model. The evolution of molar concentration for each constituent was used to analyze the initiation and develop of the reaction–diffusion process at microscale and mesoscale, from which the reaction efficiency was finally derived at macroscale. The calculated results showed that the reaction–diffusion process was significantly influenced by loading conditions, including particle velocities and loading periods. The intensification of loading conditions accelerated the consumption of reactants and the generation of reaction products. The reaction efficiency was a time-dependent parameter, which continued growing even when the shock wave had propagated through the materials. A reasonable agreement between the experimental and calculated results based on the multiscale model was achieved. Moreover, the temperature, the shock pressure, as well as the shock velocity, were found increased by the SICR behavior.

Handling Editor: Catalin Croitoru.

Address correspondence to E-mail: lynx@mail.njust.edu.cn

## Introduction

Energetic structural materials (ESMs) are commonly made up of multiple components, which possess dual functions of structural and energetic characteristics. Complicated processes, such as plastic deformation, collision and mixing between particles, pore collapse, as well as temperature rise occur in ESMs under shock conditions. Recently, extensive researches focused the mechanism of chemical reactions due to such physical processes [1–3]. Al/Ni composites is one of the typical ESMs, which composes of two material components and experiences multi-component solid-state reaction during shock compression [4, 5]. Extensive experiments [2, 3, 6] revealed that the microstructures, including particle sizes, shapes and distributions, have significant effects on SICR behavior in ESMs. Theoretical models, such as the thermochemical model [7, 8], are insufficient for describing such difference caused by microstructural effects. Instead, multiscale analysis becomes an efficient method to study the shock response of ESMs and giving reference on designing the materials.

Austin et al. [9, 10], Eakins et al. [11, 12], Smith et al. [13–15], as well as our previous work [16, 17] established mesoscale model to simulate the shock compression process in Al/Ni composites, which only considers the dynamic behavior of the composite. The aim of the above researches was to analyze the mechanism of shock reaction based on the deformation of particles and the temperature rise due to shock compression; however, the further coupling effects of shock reaction on dynamic parameters cannot be well described. Therefore, a microscopic or mesoscopic model considering reaction process is essential to make more accurate description on shock response of ESMs. It has been widely believed that the chemical reaction occurs at the interfaces between reactants when the temperature reaches a critical value. The reaction product layer at the interfaces then acts as a barrier preventing the reactants from interacting [18]. The further reaction between reactants was commonly described by introducing the mass diffusion mechanism in present models. As a result, the subsequent reaction in Al/Ni composites was maintained based on the two following processes: (1) the severe deformation of particles promotes more contacts among reactants; (2) the mass

diffusion between Al and Ni particles makes reactants transported into each other through the reaction product at Al–Ni interfaces. Due to the lack of experimental data for the coefficients of transport model during shock loadings, the present researches could be classified into two categories according to two different assumptions on the transport rate.

Do et al. [18, 19] assumed that the transport rate approximates an infinite value and the extent of reaction isn't limited by the transport mechanism. As a result, a computational method to model the shock reactions in multi-material solid powder mixtures (Nb/Si) was established. Based on this assumption, Qiao et al. [20] derived the extent of chemical reactions immediately from the impact temperature rise results by employing a thermochemical model. The infinite-transport-rate assumption maybe appropriate under the circumstance that the reaction completes on the short time scales with shock propagation, which, however, would be invalid for sufficiently coarse powder mixtures by limitation of the product barrier [18].

On the other hand, researchers such as Lomov et al. [21], Reding et al. [22, 23] and Siva et al. [24] believed the transport rate is still limited under shock conditions. Lomov et al. [21] investigated the shock reaction behavior of a mixture of spherical 2  $\mu\text{m}$  Al and 3  $\mu\text{m}$  Ni by considering the diffusion-limited process with the Arrhenius pre-exponent factor of the diffusion coefficient  $D_0 = 5 \times 10^{-8} \text{ m}^2 \text{ s}^{-1}$ . Furthermore, Reding et al. [22, 23] combined the transport rate with temperature and states of stress of constituents at the contact sites and proposed a heterogeneous chemical reaction model, which was demonstrated for Al/Ni and Al/Fe<sub>2</sub>O<sub>3</sub> powder mixtures with particle sizes below 1  $\mu\text{m}$ . As to ESMs with larger particle sizes, Siva et al. [24] proposed a “pseudo-diffusion” model with assumption of high diffusion. The value of  $D_0$  was calculated to be 10–35  $\text{m}^2 \text{ s}^{-1}$  for completion of the reaction between Nb and Si particles with size of 30–50  $\mu\text{m}$  at 800 K. Besides, molecular dynamics simulation is also an efficient method to analyze the SICR in ESMs at nanoscale [25–29].

Our previous study on Al/Ni multilayered composites with 3–5 rolling passes [16] revealed a much larger dimension on particle sizes. The layer thickness of Ni and the bilayer spacing were measured greater than 100  $\mu\text{m}$ , while the length of the layers reached millimeter level. Our experimental results also demonstrated that such Al/Ni multilayered

composites reacted fiercely at impact loadings. Therefore, both the infinite-transport-rate assumption and the limited transport rate related parameter  $D_0$  used in small dimension models (with particle size below 10  $\mu\text{m}$ ) may cause deviations in describing the shock reaction process in the Al/Ni multilayered composites. Although the RAVEN code, a two-dimensional multi-material Eulerian hydrocode, was used in simulating the dynamic response of ESMs by most researchers [9, 11, 18, 22, 23, 30], a more commonly used simulation tool is necessary to be developed to investigate the SICR mechanism of ESMs. Furthermore, the capability to have a direct comparison with experimental data at the same time and length scales is still a challenge [31].

The present paper proposes a multiscale method to study the shock reaction process in Al/Ni composites, which includes single Al and Ni particles at microscale, particle groups at mesoscale and the homogeneous material at macroscale. The Al/Ni multilayered composite with 3 rolling passes, one of typical Al/Ni composites possess large layer thickness (approaching to 200  $\mu\text{m}$ ), was selected for demonstration. Calculation results based on one-dimension reaction diffusion model were coupled with the impact initiation experiments to determine the two critical parameters in the reaction–diffusion model. The influences of heating period on the mass diffusion and the reaction process between single Al and Ni particles were analyzed by the one-dimension reaction diffusion model, which was related to the loading period. Furthermore, the SICR in the Al/Ni composite was simulated based on the reaction–diffusion model. The initiation and development of chemical reactions were analyzed by the mesoscale model, while the evolution of shock parameters and reaction efficiency at macroscale were obtained based on the mesoscale simulation results. Moreover, the influences of temperature, the shock pressure, as well as the shock velocity by shock reaction were analyzed.

## Materials and methods

### Material

The Al/Ni composite used in this work was fabricated by cold rolling with Al and Ni foils initially 0.8 mm and 0.5 mm thick, respectively. The initial Al

and Ni foils were assembled alternately and rolled to achieve sufficient deformation. Then the rolled composites were annealed in an inert atmosphere at a temperature of 550  $^{\circ}\text{C}$ . The deformed sheet was cut into two pieces and stacked by repeating the above process twice. Finally, the Al/Ni multilayered composite with 94.2% theoretical maximum density was obtained. The microstructure of the Al/Ni composite was obtained by scanning electron microscopy (SEM), as shown in Fig. 1. The Al/Ni composite revealed large particle sizes of hundreds of micrometers.

The SICR characteristics of the Al/Ni composite had been investigated in our previous work based on the two-step impact initiation experiment [16]. The relationship between the released chemical energy per gram  $e_r$  and the impact velocity  $V$  was obtained from the experiment to evaluate the energy release capacity of the material, which are listed in Table 1. Such experimental results could be used to validate the numerical results in this paper. The chemical energy of the Al/Ni composite for complete reaction  $Q_R$  was measured as 2.04  $\text{kJ g}^{-1}$  based on the fitting  $e_r$ - $V$  curve. Therefore, the reaction efficiency could be calculated as  $\eta = e_r/Q_R$ . Besides, the particle velocities corresponding to different impact velocities could be derived obeying the Hugoniot relationships between the Al/Ni composite and the steel anvil target [7]. The experimental results reveal that the chemical reaction can be initiated at  $U_p$  exceeds 437  $\text{m s}^{-1}$  and the reaction efficiency reaches 0.76 when  $U_p = 771 \text{ m s}^{-1}$ .

### One-dimension modeling

In order to describe the mass diffusion and reaction process in Al/Ni composites, a one-dimension

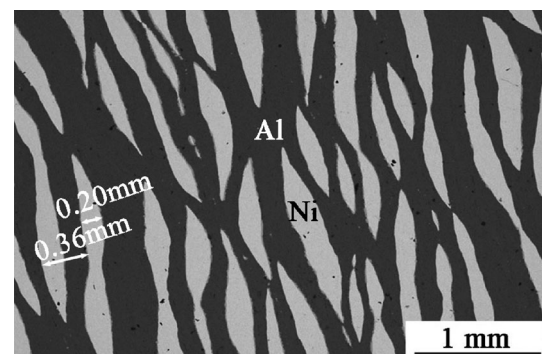


**Figure 1** The microstructure of the Al/Ni composite [16].

**Table 1** The experimental results of reaction efficiency for Al/Ni multilayered composites with 3 passes [16]

$V$ (m s <sup>-1</sup> )	$U_p$ (m s <sup>-1</sup> )	$e_r$ (KJ g <sup>-1</sup> )	$y$
841	437	0.06	0.03
872	457	0.17	0.08
1103	587	1.16	0.57
1382	771	1.55	0.76

reaction diffusion model is established firstly. The one-dimension reaction–diffusion model was established on reactants Ni and Al with the same length of  $d$ , to simulate the reaction–diffusion process between particles with finite sizes, as is shown in Fig. 2. The origin of coordinates ( $x = 0$ ) was set at the original interface between the two reactants.

The diffusion process in Al/Ni composites is described by Fick’s second law:

$$\frac{\partial C}{\partial t} = D \nabla^2 C = D \left( \frac{\partial^2 C}{\partial x^2} + \frac{\partial^2 C}{\partial y^2} + \frac{\partial^2 C}{\partial z^2} \right) \tag{1}$$

where  $t$  is time; ( $x, y, z$ ) denotes the coordinate position in a three-dimension space;  $C$  is the molar concentration for each constituent,  $D$  is a temperature-dependent diffusion coefficient. The two parameters, namely  $C$  and  $D$ , are defined as

$$D = D_0 \exp\left(-\frac{E_d}{R_u T}\right) \tag{2}$$

$$C = \hat{m} \bar{\rho} / M \tag{3}$$

where  $D_0$  is the Arrhenius pre-exponent factor of the diffusion coefficient;  $E_d$  is the activation energy for diffusion;  $R_u$  is the universal gas constant;  $T$  is temperature;  $\hat{m}$  and  $M$  are the mass fraction and molar mass for each constituent, while  $\bar{\rho}$  is the volume fraction average density. Since the activation energy for the diffusion of Ni into Al is less than half as that for the reversed diffusion, the former diffusion

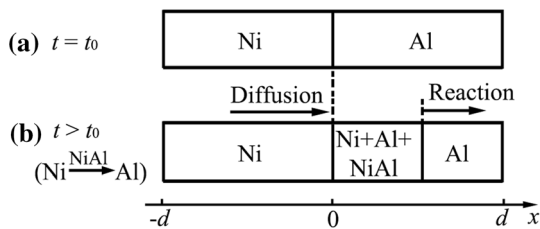


**Figure 2** Scheme of one-dimension reaction–diffusion model.

process with  $E_d = 28.0$  kJ mol<sup>-1</sup> [21] was only considered.

The corresponding one-dimension diffusion process can be described by

$$\frac{\partial C}{\partial t} = D \frac{\partial^2 C}{\partial x^2} \tag{4}$$

Chemical reaction takes places with the mass transport of Ni into Al, which causes the reduction of the molar concentration of reactants. In order to simplify the calculation process, only single-step reaction is considered, i.e.



As a result, a mixture state of Ni, Al and NiAl will occur at the right of the initial Ni–Al interface.

The reaction rate is given by [24]:

$$R = \frac{dy}{dt} = k_f C_{\text{Ni}} C_{\text{Al}} \tag{6}$$

where  $C_{\text{Al}}$  and  $C_{\text{Ni}}$  denote the molar concentration of reactants Al and Ni, respectively;  $k_f$  is the reaction rate constant, which is generally defined by the Arrhenius form as

$$k_f = A \exp\left(-\frac{E_a}{R_u T}\right) \tag{7}$$

where  $A$  and  $E_a$  are the pre-exponent factor and the activation energy for chemical reaction. The reaction rate is also corresponding to the evolution of each constituent.

According to the law of conservation of mass, the change in the molar concentration of each constituent is contributed by the concentration gradient and the chemical reaction. Therefore, the evolution of the molar concentration of Ni, Al and NiAl can be described by the reaction–diffusion equation

$$\frac{\partial C_{\text{Ni}}}{\partial t} = D \frac{\partial^2 C_{\text{Ni}}}{\partial x^2} - k_f C_{\text{Ni}} C_{\text{Al}} \tag{8}$$

$$\frac{\partial C_{\text{Al}}}{\partial t} = -k_f C_{\text{Ni}} C_{\text{Al}} \tag{9}$$

$$\frac{\partial C_{\text{NiAl}}}{\partial t} = k_f C_{\text{Ni}} C_{\text{Al}} \tag{10}$$

The initial conditions are



$$\begin{aligned}
 C_{Ni}(-d \leq x < 0, t = 0) &= C_{Ni0} \\
 C_{Al}(0 < x \leq d, t = 0) &= C_{Al0} \\
 C_{Ni}(0 < x \leq d, t = 0) &= C_{Al}(-d \leq x < 0, t = 0) = 0 \\
 C_{NiAl}(x, t = 0) &= 0
 \end{aligned}
 \tag{11}$$

The boundary condition is

$$C_{Ni}(x < -d, t) = 0
 \tag{12}$$

### Mesoscale modeling

#### Numerical simulation model

Based on the above one-dimension reaction–diffusion model, the shock reaction process in Al/Ni composites was studied on mesoscale by using ABAQUS. The modeling process is shown in Fig. 3. A typical area marked with a yellow rectangle in Fig. 3a was selected to establish the mesoscale model. The direction of the Al/Ni layers was adjusted to keep perpendicular to the load direction, according to the actual manufacturing process and experimental setup. In order to investigate the shock reaction process, the selected area was extended by translating the microstructure along the propagation direction of the shock wave, as shown in Fig. 3b. The length and the width of the computational model were 5.5 mm and 2.75 mm, respectively. The thickness of the model was set as only 0.01 mm, to simulate the 1-D process of shock wave propagating in one of cross sections of the Al/Ni composite.

According to the one-dimension reaction–diffusion model, the exact positions for each material point and interface are essential in calculations. Lagrange algorithm, instead of Eulerian algorithm, is selected to simulate the mass diffusion and chemical reaction in the Al/Ni composite, due to its advantage that

only single material existing in one element. Eight-node linear brick element with reduced integration was used and the mesh size was set as 0.01 mm. Typical mesh of the model is shown in Fig. 3c. A rigid plate was established on the left hand of the mesoscale model with constant velocities from  $350 \text{ m s}^{-1}$  to  $900 \text{ m s}^{-1}$ , which is equal to the particle velocity  $U_p$  in the Al/Ni composite. The mesh size of the rigid plate is 0.01 mm. Each side of the Al/Ni model except the loading side was prescribed with symmetric conditions to simulate a periodic microstructure and the 1-D shock compression process.

#### Modeling the dynamic response and shock reaction process in the Al/Ni composite

**Equation of state (EOS)** The Al and Ni particles were regarded as fluid to study their dynamic response under shock conditions, where the resistance to shear could be omitted. The constitutive model of the two materials is simplified as the relationship between the hydrostatic stress and the specific volume, namely the EOS for high pressure solids. The shock compression is assumed as an adiabatic process, during which the heat dissipation is not considered.

The Mie–Grüneisen EOS [32] was used to calculate the shock response of materials, which is defined in the form of:

$$P - P_H = \gamma \rho (E - E_H)
 \tag{13}$$

where  $P_H$  and  $E_H$  are the Hugoniot pressure and specific energy;  $\gamma$  is the Grüneisen coefficient;  $\rho$  is the density of materials.

The relationship between particle velocity ( $U_p$ ) and shock velocity ( $U_s$ ) is commonly described in a linear form of [33]:

$$U_s = C_0 + S U_p
 \tag{14}$$

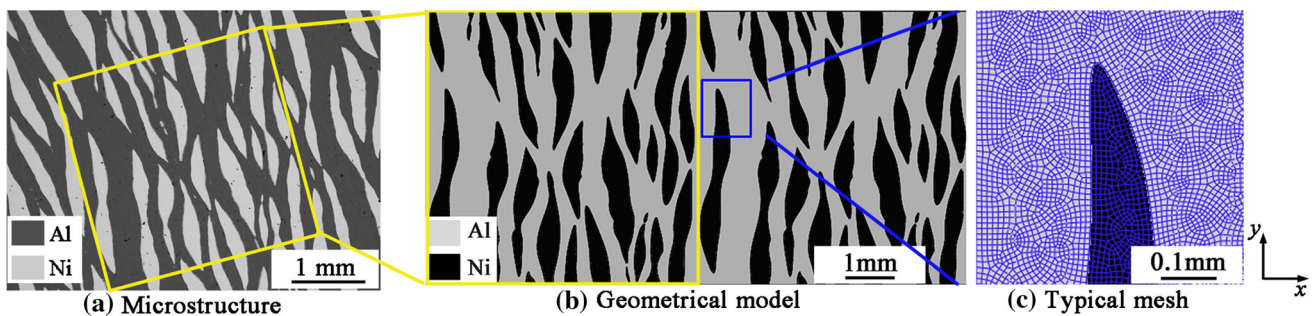


Figure 3 The microstructure, the geometrical model and partial meshes of the model.

where  $C_0$  is the sound speed in material;  $S$  is a material constant. The EOS parameters of Al and Ni are listed in Table 2.

**Modeling the shock reaction process based on reaction–diffusion model** The user subroutine VUMAT in ABAQUS is used to define the dynamical behavior and shock reaction of Al/Ni composites. The VUMAT routine is written based on the shock EOS and the reaction–diffusion model. The calculation flow chart is illustrated in Fig. 4, which can be separated into the following three steps:

Based on the Mie–Grüneisen EOS, the stress in the materials due to shock compression can be calculated. The rate of change in specific internal energy is defined by

$$\dot{E} = \frac{\sigma : \dot{\epsilon}}{\rho} \tag{15}$$

where  $\sigma$  and  $\dot{\epsilon}$  are the stress tensor and strain rate tensor at materials points, respectively. According to the adiabatic assumption, the temperature rise is mainly controlled by the plastic work dissipation on the mechanical aspect, which is written as

$$\dot{T} = \frac{\sigma : \dot{\epsilon}}{\rho C_p} \tag{16}$$

where  $\dot{T}$  is the temperature rate;  $C_p$  is the specific heat capacity of materials, which equals  $903 \text{ J kg}^{-1} \text{ K}^{-1}$ ,  $444 \text{ J kg}^{-1} \text{ K}^{-1}$  and  $540 \text{ J kg}^{-1} \text{ K}^{-1}$  for Al, Ni and NiAl [16, 21], respectively.

The molar concentration gradient exists along two directions, namely  $x$  and  $y$ , in the numerical model. Therefore, a two-dimension mass diffusion process takes places during the shock compression. Before solving the two-dimension form of diffusion–reaction Eqs. (10)–(14), the coordinates of material points were extracted and written in a file from ABAQUS. Then the adjacent point pairs were matched from the file, on condition that the distance between each other below the average value. Afterwards, the molar concentrations of constituents between the adjacent

**Table 2** EOS parameters of Al and Ni [16, 21, 33]

Materials	$\rho/(\text{kg m}^{-3})$	$C_0/(\text{m s}^{-1})$	$S$	$\gamma$
Al	2784	5370	1.29	2.18
Ni	8875	4590	1.44	2.00

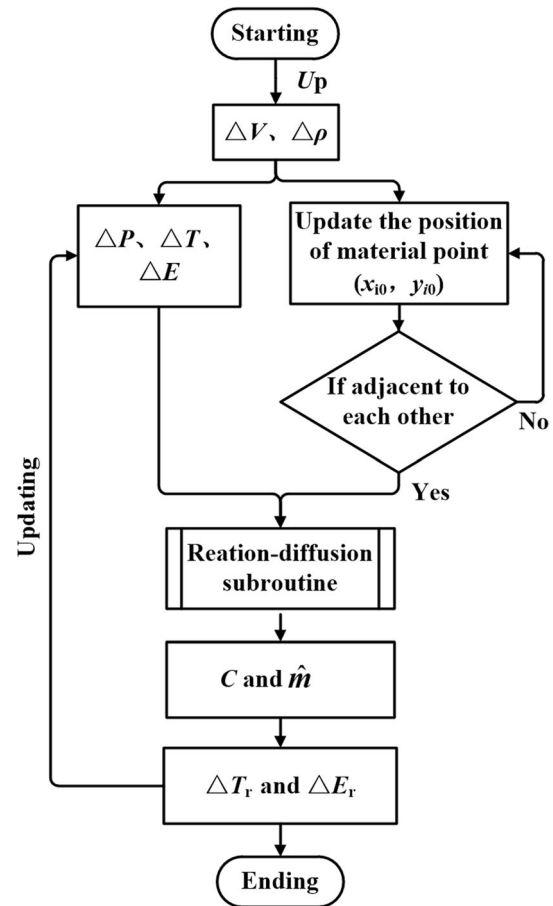


**Figure 4** The flow chart to calculate the dynamic response and shock reaction in the Al/Ni composite.

points were updated according to their present values and the average temperature of the point pairs. The mass fraction of constituents at materials points were calculated by Eq. (3).

Chemical energy will be released when the reaction is initiated, which can cause the increase of the system energy and temperature. Therefore, the two variables ( $E'$  and  $T'$ ) at material points were updated according to the corresponding increments ( $E_r$  and  $T_r$ ) from shock reaction.

$$\dot{E}' = \dot{E} + \dot{E}_r = \dot{E} + Q_R \frac{d\hat{m}_{NiAl}}{dt} \tag{17}$$

$$\dot{T}' = \dot{T} + \dot{T}_r = \dot{T} + \frac{Q_R}{C_p} \frac{d\hat{m}_{NiAl}}{dt} \tag{18}$$

where  $Q_R$  is the chemical energy per unit mass for complete reaction. This paper is concentrated on the mechanism for shock reaction in Al/Ni composites and the influence of the reaction on shock parameters. The material parameters for the constituents were not updated for simplification.

## The evolution of reaction efficiency based on mesoscale simulation

The ultimate aim of this work is to obtain macroscale characteristics considering mesoscopic effects, where both the evolution of the reactions and shock waves play important roles. In the aspect of chemical reaction, the reaction efficiency at the following three typical areas will be calculated to make such analysis: (1) the first one is the reaction efficiency at a typical area where the  $x$  coordinate is less than 0.5 mm, which represents the evolution of reaction at specific area (near the loading side) during shock compression; (2) the second one is the reaction efficiency in the entire mesoscale model, which represents the evolution of reaction in the material with specific size (equalling to the size of the mesoscale model); (3) the last one is the reaction efficiency behind the shock front, which is independent of the size of the materials and can reveal the macroscopic reaction evolution in energetic materials. On the other hand, the Hugoniot parameters will be calculated to analyze the evolution of shock waves accompanied with chemical reaction.

In order to calculate the reaction efficiency, the first step is to extract the total mass of the reaction products  $m_{\text{NiAl}}$  during shock reactions, which could be defined by the sum of which in each element at specific areas:

$$m_{\text{NiAl}} = M_{\text{NiAl}} \sum (\Delta C_{\text{NiAl}} \Delta V) \quad (19)$$

where  $\Delta C_{\text{NiAl}}$  is the molar concentration of NiAl in an element;  $\Delta V$  is the volume of an element.

As a result, the reaction efficiency can be calculated by the proportion of the mass of reaction products  $m_{\text{NiAl}}$  to the total mass of the initial reactants  $m_0$  at specific areas:

$$y = m_{\text{NiAl}}/m_0 \quad (20)$$

## Results and discussion

### Analysis on reaction–diffusion process between single Al and Ni particle

Based on the one-dimension reaction–diffusion model, the diffusion and reaction between single Al and Ni particles at specific temperature can be predicted. Here, the length of constituents  $d$  is set to

200  $\mu\text{m}$ , which is similar to the layer thickness of Al/Ni multilayer composites. The molar mass  $M$  and the initial density  $\rho$  of Ni, Al and NiAl, as well as activation energy for mass diffusion and reaction are listed in Table 3.

### Determination of reaction–diffusion parameters

The Arrhenius pre-exponent factor of the diffusion coefficient  $D_0$  and the pre-exponent factor for chemical reaction  $A$  are two critical parameters related to the mass diffusion rate and chemical reaction rate, respectively. The value of  $D_0$  was determined as  $5 \times 10^{-8} \text{ m}^2 \text{ s}^{-1}$  by shear-cell technique [21]. However, this value is not applicable to predict the diffusion results under shock conditions [22–24]. On the other hand, Lomov et al. [21] calibrated that  $5 \times 10^9 (\text{mol m}^{-3})^{-1} \cdot \text{s}^{-1}$  could be used as value of  $A$  to simulate the reaction in Al/Ni nano-laminate within 150 ns. Actually, the period for shock waves propagating in an Al/Ni specimen in impact initiation experiments exceeds 1  $\mu\text{s}$ . In order to determine the two reaction–diffusion parameters, one-dimension reaction–diffusion calculations were conducted with different values of  $D_0$  and  $A$ .

Shock compression causes the rise of temperature in reactive materials, which can lead to the shock reaction of the material. The shock reaction efficiency is controlled by the shock conditions [8]. In order to determine the reaction–diffusion parameters, two values of temperatures, i.e., 700 K and 1500 K, were used in the calculations, which are approximated to the temperature response at Al–Ni interfaces with particle velocities of 437  $\text{m s}^{-1}$  and 771  $\text{m s}^{-1}$ , respectively. The heating period was set as 1  $\mu\text{s}$  and the calculation results are illustrated in Fig. 5. For convenience, the area left to the interface which was initially occupied by Ni was defined as  $x^-$ , while the area initially occupied by Al was defined as  $x^+$ . It is shown that the mass transport of Ni reduced its molar concentration in the area  $x^-$ , while the chemical reaction reduced the molar concentration of the two reactants and increased that of the chemical product NiAl in the area  $x^+$ . As a result, a mixture of Al, Ni and NiAl was produced in the area  $x^+$  close to the interface.

The molar concentration of Ni is controlled by both mass diffusion and chemical reaction. As the mass diffusion was initialized at the interface and Ni was transported from  $x^-$  to  $x^+$ , the molar concentration of

**Table 3** Material parameters of Ni, Al and NiAl

$M$ (g mol <sup>-1</sup> )			$\rho$ (g cm <sup>-3</sup> )			$E_d$ (KJ mol <sup>-1</sup> )	$E_a$ (KJ mol <sup>-1</sup> )
Ni	Al	NiAl	Ni	Al	NiAl		
58.7	27	85.7	8.875	2.784	5.173	28 <sup>a</sup>	88.6 <sup>a</sup>

<sup>a</sup>Obtained from Refs [21]

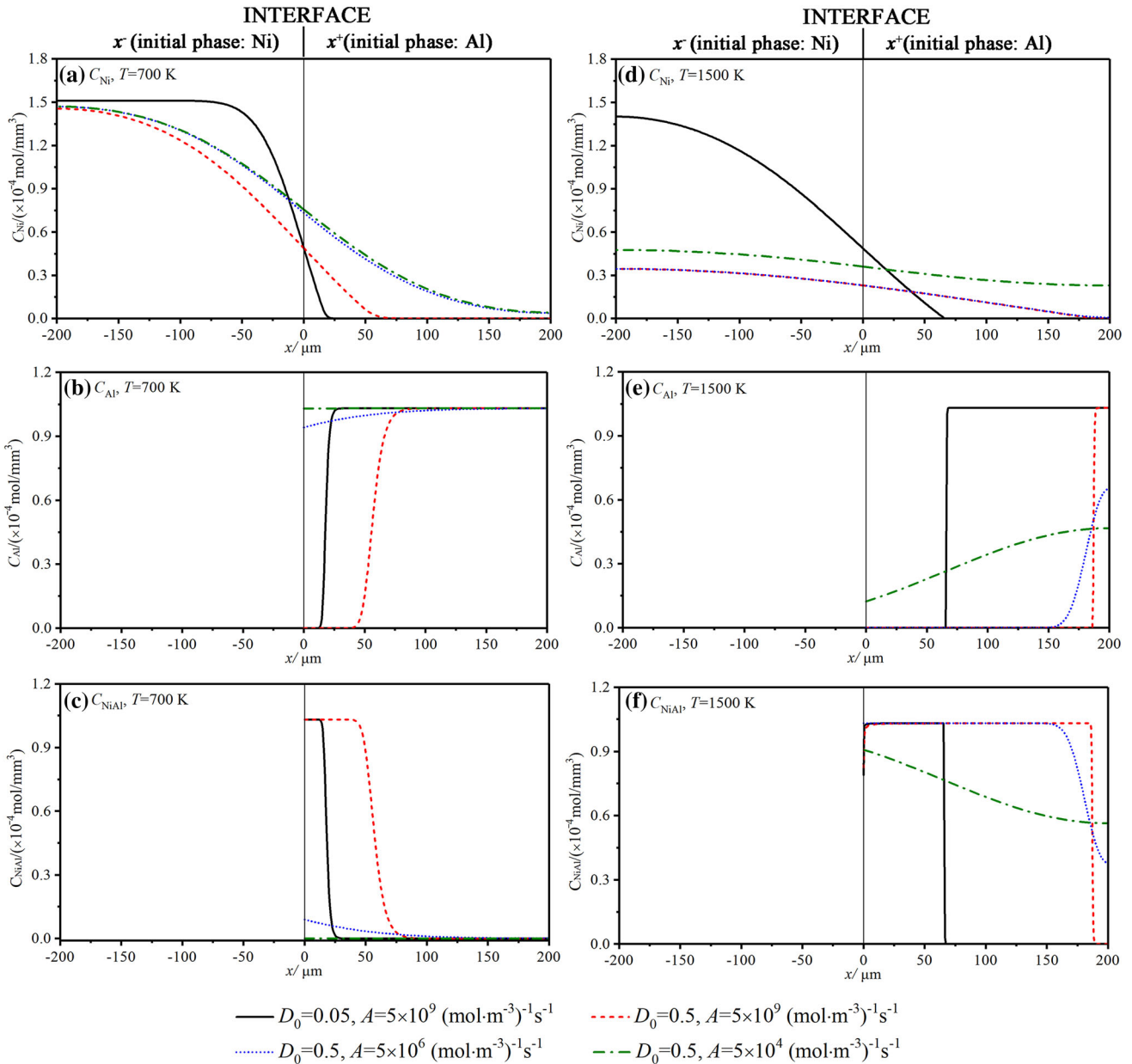


**Figure 5** The one-dimension reaction–diffusion results with different  $D_0$ .

Ni reveals a decreasing trend along the axis direction. It was found from the calculations that the reaction–diffusion process only took place within 1  $\mu\text{m}$  away from the Al–Ni interface at 1500 K with  $D_0 = 5 \times 10^{-8}$

$\text{m}^2 \text{s}^{-1}$  and  $A = 5 \times 10^9 (\text{mol}\cdot\text{m}^{-3})^{-1}\cdot\text{s}^{-1}$ , which was not illustrated in Fig. 5. This means that the value of  $D_0$  should be enlarged to ensure the transport of Ni to farther position in the area  $x^+$  to support the reaction



process. When  $D_0$  equaled  $0.05 \text{ m}^2 \text{ s}^{-1}$  and  $0.5 \text{ m}^2 \text{ s}^{-1}$ , the chemical reaction at 1500 K extended to the position where  $x$  approximated to  $66 \text{ }\mu\text{m}$  and  $190 \text{ }\mu\text{m}$ , respectively. Therefore, the value  $0.5 \text{ m}^2 \text{ s}^{-1}$  is applicable for  $D_0$  to describe the mass diffusion process in the Al/Ni multilayered composite.

Furthermore, the distribution of the molar concentration of Al and NiAl can directly reflect the reaction efficiency, as the contents of the two constituents can be only controlled by chemical reaction process. At the circumstance that  $D_0 = 0.5 \text{ m}^2 \text{ s}^{-1}$  and  $A = 5 \times 10^9 \text{ (mol}\cdot\text{m}^{-3})^{-1} \text{ s}^{-1}$ , the molar concentration of Al where  $x$  was below  $40 \text{ }\mu\text{m}$  equaled zero at 700 K, which means that the reactant Al in this area was exhausted by chemical reaction. This result deviated significantly from the experimental data that the reaction efficiency was closed to zero at  $U_p$  exceeds  $437 \text{ m s}^{-1}$ . Therefore, the value of  $A$  should be minished to ensure the reaction rate to be small enough at 700 K. When  $A$  was reduced to  $5 \times 10^6 \text{ (mol}\cdot\text{m}^{-3})^{-1}\cdot\text{s}^{-1}$ , the molar concentration of Al was decreased slightly near the interface at 700 K and consumed in quantity at 1500 K. If the value of  $A$  was further reduced to  $5 \times 10^4 \text{ (mol}\cdot\text{m}^{-3})^{-1}\cdot\text{s}^{-1}$ , the reaction rate was too slow to support the reaction at 1500 K. Therefore, the value  $5 \times 10^6 \text{ (mol}\cdot\text{m}^{-3})^{-1}\cdot\text{s}^{-1}$  is applicable for  $A$  to describe the mass diffusion process in the Al/Ni multilayered composite. Besides, NiAl was produced with the consuming of Al and the molar concentration of NiAl shows a significantly increasing trend with the increase of the temperature.

#### *Reaction–diffusion process in Al/Ni particles for different heating period*

According to Eqs. (8)–(10), the extent of mass diffusion and chemical reaction are related to the heating period. The investigation on the influence of heating period on the reaction–diffusion process can help to understand the chemical reaction process during shock compression. Therefore, the distribution of molar concentration of each constituent after  $0.2 \text{ }\mu\text{s}$  to  $1.5 \text{ }\mu\text{s}$  at 1500 K is calculated, as shown in Fig. 6.

It's shown that the molar concentrations of the two reactants, Ni and Al, decline significantly from  $0.2 \text{ }\mu\text{s}$  to  $1.5 \text{ }\mu\text{s}$  at their original area, while NiAl grows quickly during the heating period. This means that the increase of heating period accelerates both the

diffusion and reaction process. Long heating period can enlarge the area referring to diffusion and reaction. The reaction only took place in the area  $x^+$  with  $x$  less than about  $50 \text{ }\mu\text{m}$  during the heating period within  $0.2 \text{ }\mu\text{s}$ , which nearly completed after  $1.5 \text{ }\mu\text{s}$  with exhausted Al at entire area. Actually, the reaction–diffusion process is more complicated among a large number of particles at mesoscale than the simple one-dimension process. The temperature and the heating period for each element are totally different. Further analysis should be conducted based on mesoscale simulations.

## Mesoscale simulation results and discussion

### *The propagation of shock waves in Al/Ni compression*

The dynamic response of Al/Ni at typical particle velocity  $U_p = 771 \text{ m s}^{-1}$  was analyzed according to the calculated pressure and temperature results, as shown in Fig. 7. With the length of the mesoscale model being compressed from  $5.5 \text{ mm}$  to  $4.81 \text{ mm}$ , the discrete Ni layers experienced severe deformation. Shock waves were produced in the Al/Ni composite, which reached the end of the model at about  $0.88 \text{ }\mu\text{s}$ . The shock pressure in Al/Ni multilayered composites approximated to  $25 \text{ GPa}$  at  $U_p = 771 \text{ m s}^{-1}$  at most region, but which exceeded  $40 \text{ GPa}$  at local small region. The impedance difference between Al and Ni and the irregular particles made contribution to the ununiformed distribution of the shock pressure.

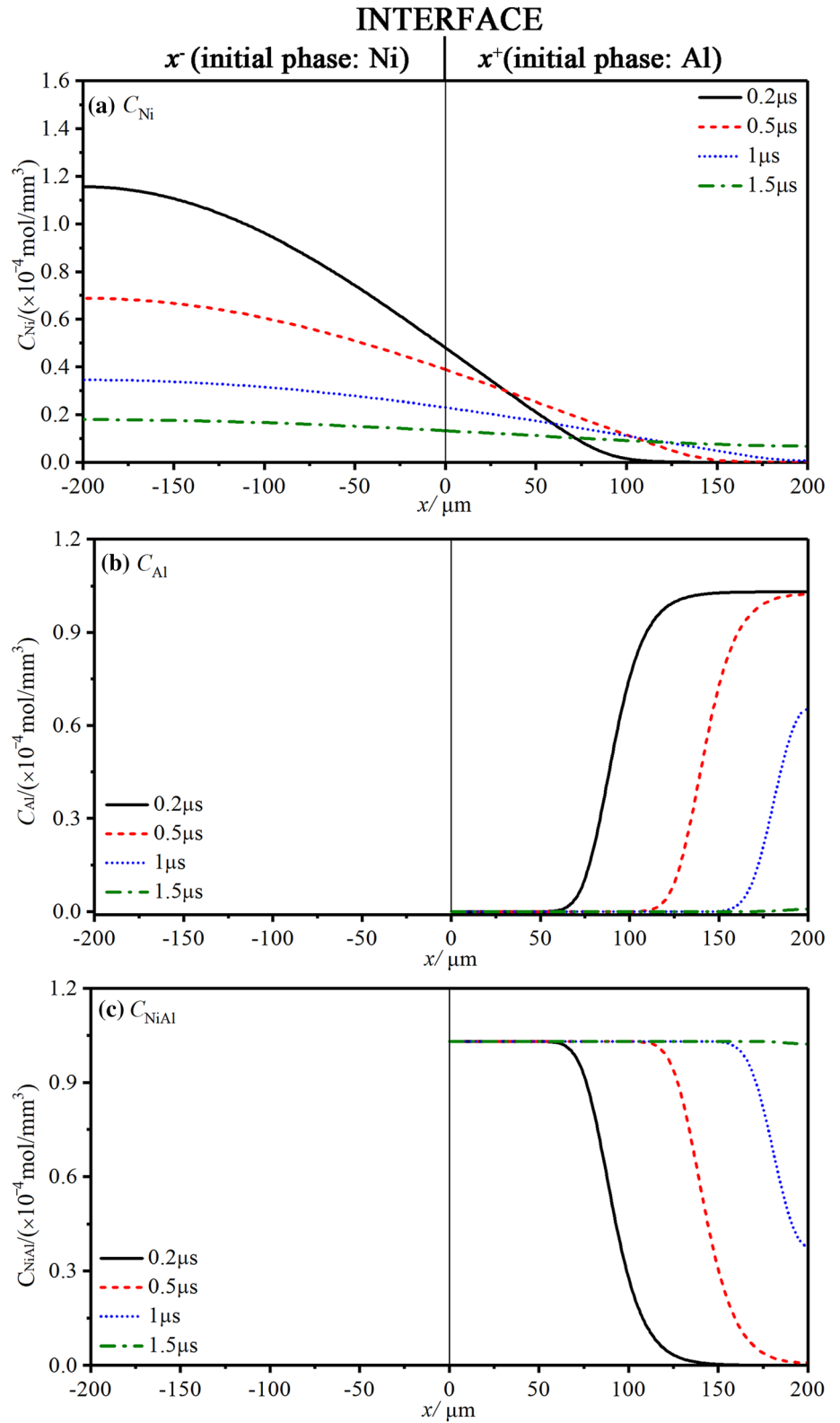
On the other hand, the temperature approximated to  $1000 \text{ K}$  at the most area and exceeded  $1800 \text{ K}$  at local region. The temperature showed a more regular distribution than pressure. The locally high temperature was produced along the Al–Ni interfaces behind shock waves, which was extended with the propagation of the shock waves. According to Eq. (18), the temperature rise was contributed by both the plastic work in shock compression and the energy released from chemical reaction. Therefore, the locally high-temperature area represents where chemical reaction occurred.

### *The reaction and diffusion process in Al/Ni composites*

*The diffusion process in Al/Ni composites* The evolution of molar concentration of Ni during shock



**Figure 6** The distribution of molar concentration of Ni, Al and NiAl for different heating period.



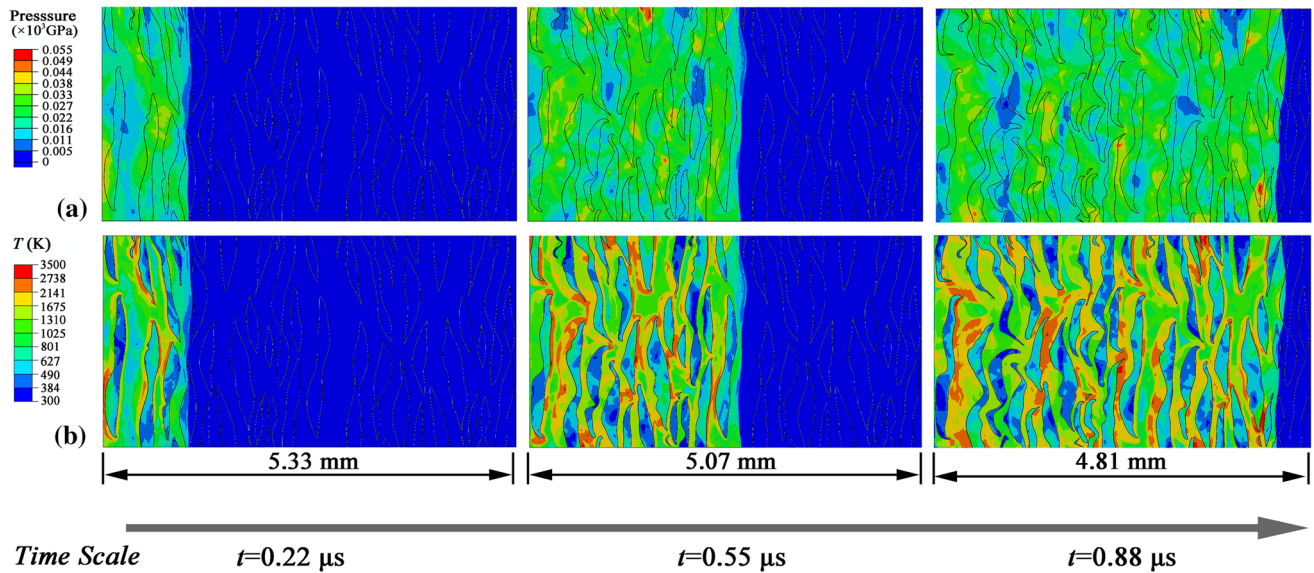


**Figure 7** The dynamic response in the Al/Ni composite: **a** shock pressure and **b** temperature.

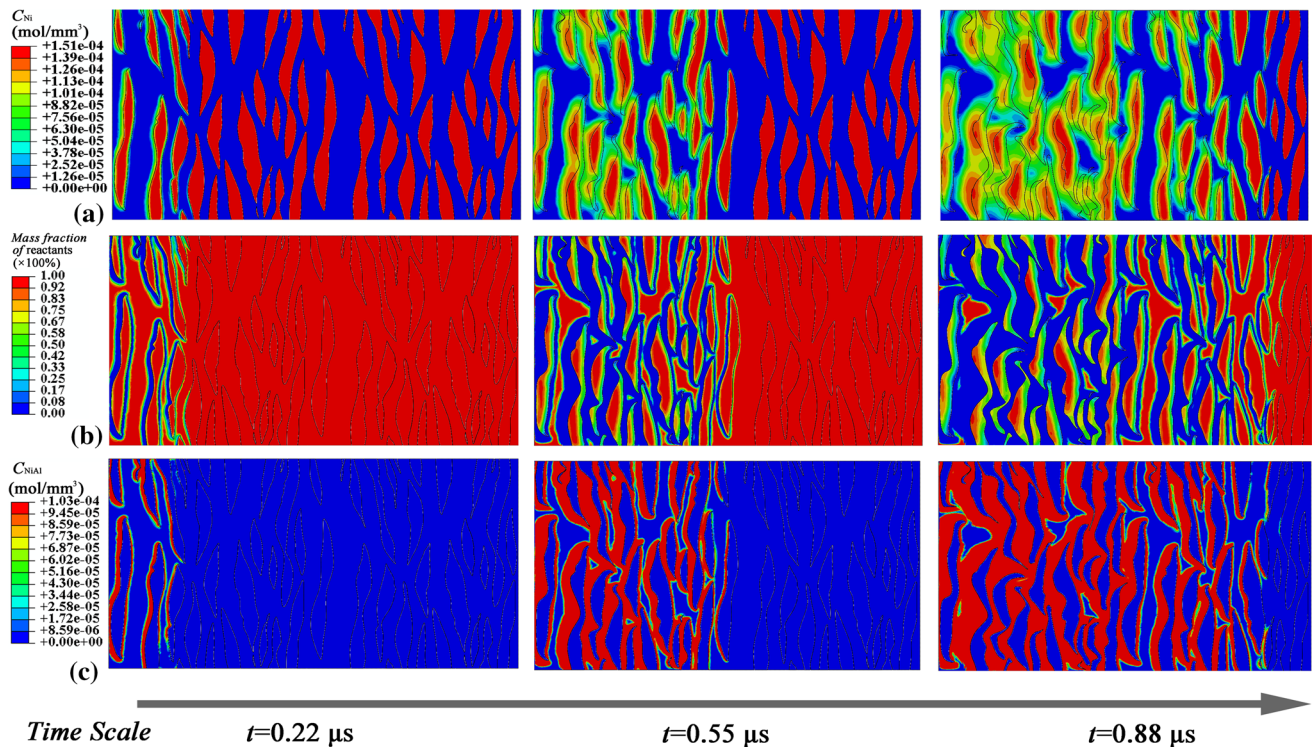


**Figure 8** The evolution of **a** Ni, **b** residual reactants and **c** reaction product at particle velocity of  $800 \text{ m s}^{-1}$ .

compression with particle velocity of  $771 \text{ m s}^{-1}$  is shown in Fig. 8a. With shock waves propagating in the Al/Ni composites, the temperature rose rapidly that caused mass diffusion between Al and Ni. The Ni constituent began to be transported into the area where had been initially occupied by Al through the first Al-Ni interfaces at  $0.22 \mu\text{s}$ . With the increase of

the loading period, the mass diffusion occurred at more Al-Ni interfaces and more Ni was transported. When the shock wave moved to the end of the composite (at about  $t = 0.88 \mu\text{s}$ ), the mass diffusion took place at most of the Al-Ni interfaces, but Ni had not been transported into the entire area initially occupied by Al. This indicates that the mass diffusion

in the Al/Ni composite with large particle size was not completed after the propagation of shock waves. The mass diffusion continued behind the shock waves.

**The reaction process in the Al/Ni composite** In order to investigate the reaction process, the variation of the constituents in the Al/Ni composite was analyzed. The consumption of the reactants can be reflected by the residual of constituents at their original domains. The distribution of the mass fraction of the reactants during shock compression is shown in Fig. 8b. Here, the mass fraction of reactants at the original domain with Al represents the mass fraction of Al. Since only one constituent exists in the original domain with Ni, the mass fraction of reactants was defined by the ratio of residual mass of Ni to its initial value. The red spectrum in Fig. 8 represents the area without any consumption of reactants, while the blue spectrum is corresponding to the area where the reactants have been exhausted. It is shown that the exhaustion of reactants occurred initially at the Al–Ni interface and then extended to both sides. The consumption of the reactants kept growing with the propagation of shock waves.

Figure 8c is the evolution of the molar concentration of the reaction product (NiAl) during shock compression. There was no reaction product in the Al/Ni composites before the shock loading. Due to the assumption that only the diffusion process of Ni into Al was considered, the reaction product could be merely produced at the original domain with Al. It can be found that the reaction product was produced firstly at the Al/Ni interface and then extended with the diffusion direction. The chemical reaction occurred around the Al particles, which resulted in the convergence of the reaction product at the center of the original domain with Al. The red spectrum means one of the reactants was exhausted and the chemical reaction would not take place any more. Compared with Fig. 7, the area with high temperature agrees well with where reaction products were produced.

#### *Effects of particle velocity on the shock response of the Al/Ni composite*

The distribution of the molar concentration of the reaction product at different particle velocities ( $t = 0.88 \mu\text{s}$ ) is shown in Fig. 9. Only the area initially occupied by Al was illustrated to analyze the

chemical reaction with greater clarity. It could be found that few reaction products were produced at the particle velocity of  $437 \text{ m s}^{-1}$ . With the increase of particle velocity, the distribution of the reaction product kept expanding. Therefore, the Al/Ni composite needs a minimum particle velocity to initiate the chemical reaction. The increase of the particle velocity could increase the reaction efficiency in the Al/Ni composite.

The shock pressure and temperature results of the Al/Ni composite at different particle velocities are shown in Fig. 10. Both the shock pressure and temperature revealed an increasing trend with the growth of particle velocities. Besides, the increasing particle velocity caused larger deformation of the particles. At the particle velocity of  $437 \text{ m s}^{-1}$ , a small number of hotspots exceeding 1300 K were formed closely to the interfaces, while the temperature at most domain was below 800 K, which is in accordance with the distribution of the reaction product in the Al/Ni composite. The increased temperature in the composites due to higher particle velocities promoted both the mass diffusion and chemical reaction. Therefore, the local high-temperature area was extended at higher of particle velocities.

### **Macroscale analysis on SICR and discussion**

#### *Analysis on the area near the loading side*

Distributions of the molar concentration of the reaction product during the shock compression with the particle velocity of  $771 \text{ m s}^{-1}$  are shown in Fig. 11. It is obvious that the original rectangle area gradually became irregular within the  $0.88 \mu\text{s}$  loading period. Bits of reaction products were produced at the first layer of Al–Ni interfaces at the beginning of the shock loading. The reaction products continued growing even when the shock wave had propagated through the right margin of the area at  $0.11 \mu\text{s}$ . At the time of  $0.88 \mu\text{s}$ , the reaction products “born” from each interface nearly grew together.

The calculated total mass of the reaction product  $m_{\text{NiAl},0.5}$  versus time curves at different particle velocities near the loading side is shown in Fig. 12. The subscript “0.5” denotes the corresponding value within the area where the  $x$  coordinate is less than 0.5 mm. It appears that an increase of loading period leads to a monotonic increase of the mass of the reaction product. At the particle velocity of



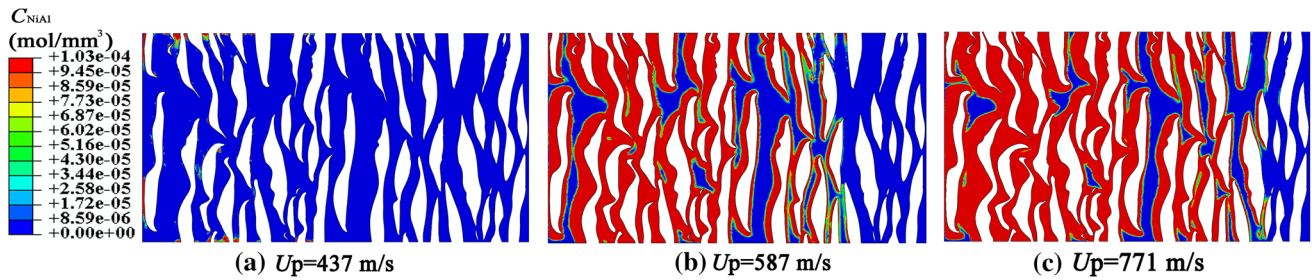


**Figure 9** The distribution of the reaction product in the Al/Ni composite at different particle velocities.

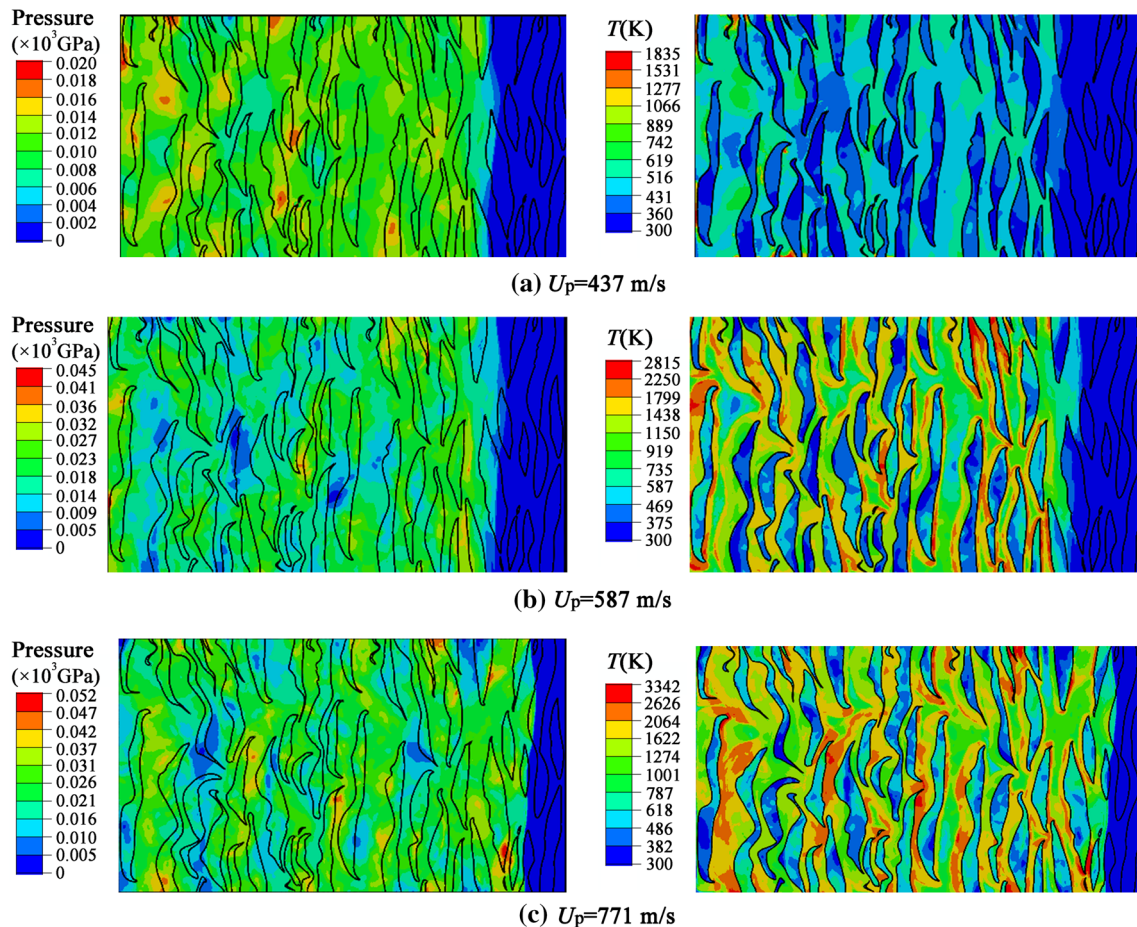


**Figure 10** The shock compression results of the Al/Ni composite at different particle velocities.

$350 \text{ m s}^{-1}$ , the values of  $m_{\text{NiAl},0.5}$  approached zero, indicating no chemical reaction took place. With increase of  $U_p$  up to  $900 \text{ m s}^{-1}$ , the mass diffusion and reaction processes were intensified, which resulted in the substantial increase of  $m_{\text{NiAl},0.5}$ . As for  $U_p = 900 \text{ m s}^{-1}$ , the reaction efficiency at  $0.88 \mu\text{s}$  is 6.3 times of that at  $0.11 \mu\text{s}$  when shock waves propagated through the right margin of the area. This calculated result indicates that the shock reaction mainly develops behind shock waves.

#### *Analysis on the entire mesoscale model*

The calculated total mass of the reaction product  $m_{\text{NiAl,meso}}$  and the reaction efficiency  $y_{\text{meso}}$  versus time curves at different particle velocities within the entire mesoscale model are shown in Fig. 13. Similarly, the two parameters increased with particle velocities due to relative intense loading conditions. During the shock compression process, the two dependent variables,  $m_{\text{NiAl,meso}}$  and  $y_{\text{meso}}$ , grew

**Figure 11** Distributions of the molar concentration of the reaction product during the shock compression with particle velocity of  $800 \text{ m s}^{-1}$ .

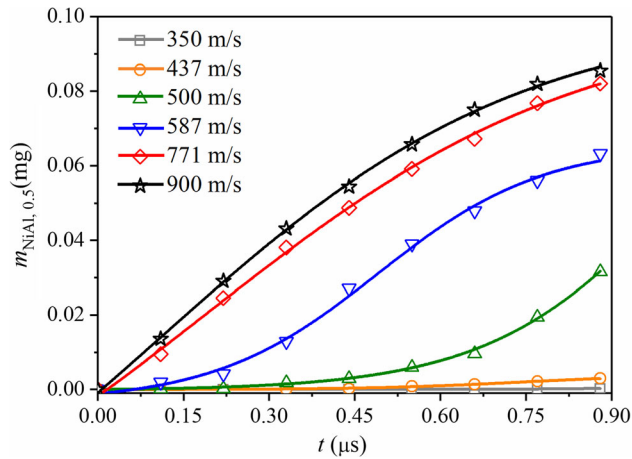
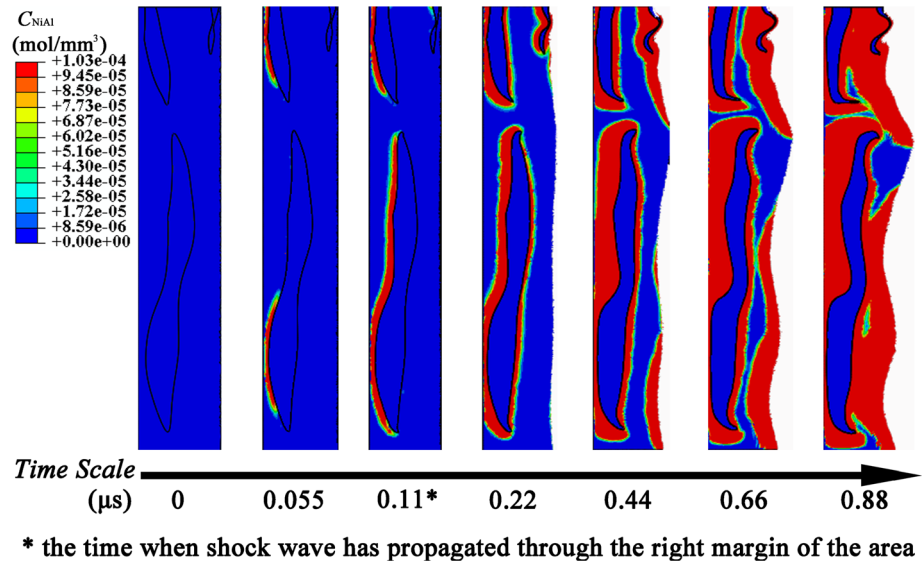


**Figure 12** The calculated total mass of the reaction product and the reaction efficiency versus time curves at different particle velocities within the area where  $x$  coordinate less than  $0.5 \text{ mm}$ .

slowly firstly and then grew fast. It also could be observed from Figs. 8c and 9 that the distribution of the reaction product had a decrease tendency along the loading direction. Furthermore, the reaction efficiency at  $U_p = 900 \text{ m s}^{-1}$  is close to which at  $U_p = 771 \text{ m s}^{-1}$ .

*Analysis on the reaction efficiency behind the shock front*

The reaction efficiency behind the shock front  $y_{\text{shock}}$  could be derived from the mass of reaction products within the mesoscale and the total mass of the initial reactants behind the shock front at specific time, which is shown in Fig. 14a. The evolution of  $y_{\text{shock}}$  represents the reaction efficiency in macroscale

materials during the shock compression process. In order to make a comparison with Al/Ni composites with smaller particle size, simulations were also conducted on powder composites with the same stoichiometric ratio of Al to Ni at  $U_p = 800 \text{ m s}^{-1}$ . The average size of the Al and Ni particles is  $0.023 \text{ mm}$  and  $0.075 \text{ mm}$ , respectively. The microstructure of the powder compaction is described in our previous work [16]. The mark “PD” denotes the powder compaction, while the mark “ML” denotes the multilayered composite. With the propagation of shock waves, the shock efficiency in materials increased steadily with the loading period, which is consistent with the regularity at mesoscale in Fig. 13. The difference is the reaction efficiency tended to grow slowly at last.

It could be found that the  $y_{\text{shock}}-t$  curve at  $U_p = 437 \text{ m s}^{-1}$  for the Al/Ni multilayered composite had low relative deviation from the base line  $y_{\text{shock}} = 0$ . Therefore,  $U_p = 437 \text{ m s}^{-1}$  could be regarded as the critical condition to initiate the chemical reaction in the Al/Ni multilayered composite. Furthermore, the  $y_{\text{shock}} - t$  curve at  $U_p = 900 \text{ m s}^{-1}$  was nearly to which at  $U_p = 771 \text{ m s}^{-1}$ . The value of  $y_{\text{shock}}$  reached 0.91 when  $t = 0.88 \mu\text{s}$  for  $U_p = 900 \text{ m s}^{-1}$ , which means  $U_p = 900 \text{ m s}^{-1}$  is approaching to the particle velocity to complete the chemical reaction. Besides, the  $y_{\text{shock}}-t$  curve of the Al/Ni powder compaction at  $U_p = 800 \text{ m s}^{-1}$  was always higher than which of the Al/Ni multilayered composite within  $0.15 \mu\text{s}$ . It could be inferred that the chemical reaction rate is



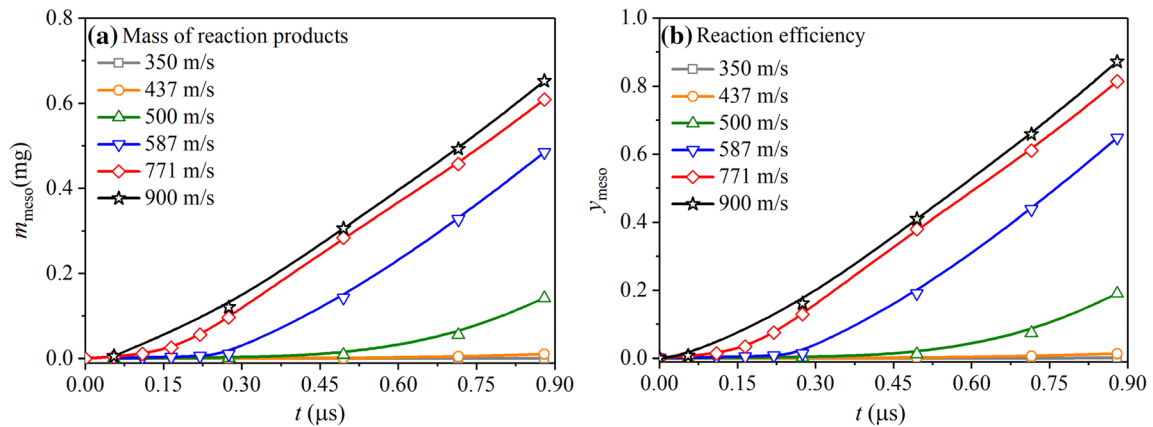


**Figure 13** The calculated total mass of the reaction product and the reaction efficiency versus time curves at different particle velocities within mesoscale model.

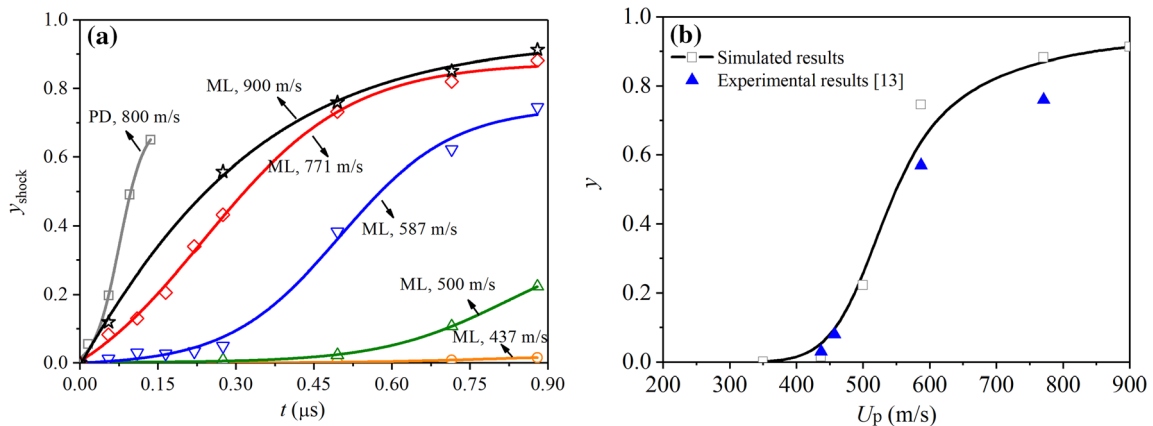


**Figure 14** The reaction efficiency behind the shock front: **a** the calculated reaction efficiency versus time curves at different particle velocities; **b** the comparison of the reaction efficiency between simulated results at different time and the experimental results [16].

higher in the Al/Ni composite with smaller particle size.

The simulated reaction efficiency versus the particle velocity curves at  $t = 0.88 \mu\text{s}$  is shown in Fig. 14b. The calculated  $\gamma-U_p$  curve shows a consistent trend with the corresponding experimental results, where the value of  $\gamma$  approximated to zero under the  $U_p$  below  $437 \text{ m s}^{-1}$  and increased with  $U_p$  once the reaction was initiated.

### The influence of chemical reaction on shock compression results

#### The influence of chemical reaction on shock pressure and temperature

Equations (17) and (18) reveal that the shock reaction could contribute to both the specific internal energy and temperature in the Al/Ni composite. In order to

investigate the influence of chemical reaction on the shock compression results, the distribution of shock pressure and shock temperature at typical time ( $t = 0.88 \mu\text{s}$ ) were analyzed. The comparison of the calculation results whether considering the shock reaction is shown in Fig. 15. At particle velocity of  $771 \text{ m s}^{-1}$ , the maximum pressure in the Al/Ni composite only caused by the mechanical response was 43 GPa. However, the value rose to 52 GPa when considering the chemical reaction. Furthermore, the shock wave propagated to the further position when reaction took place, which indicates that the reaction could accelerate the shock velocity. On the other hand, the chemical reaction increased the maximum temperature in the Al/Ni composites significantly by 1403 K. It is obvious that the hotspots, with larger temperature than the maximum value in Fig. 15a, were distributed around the Al-Ni interfaces in the

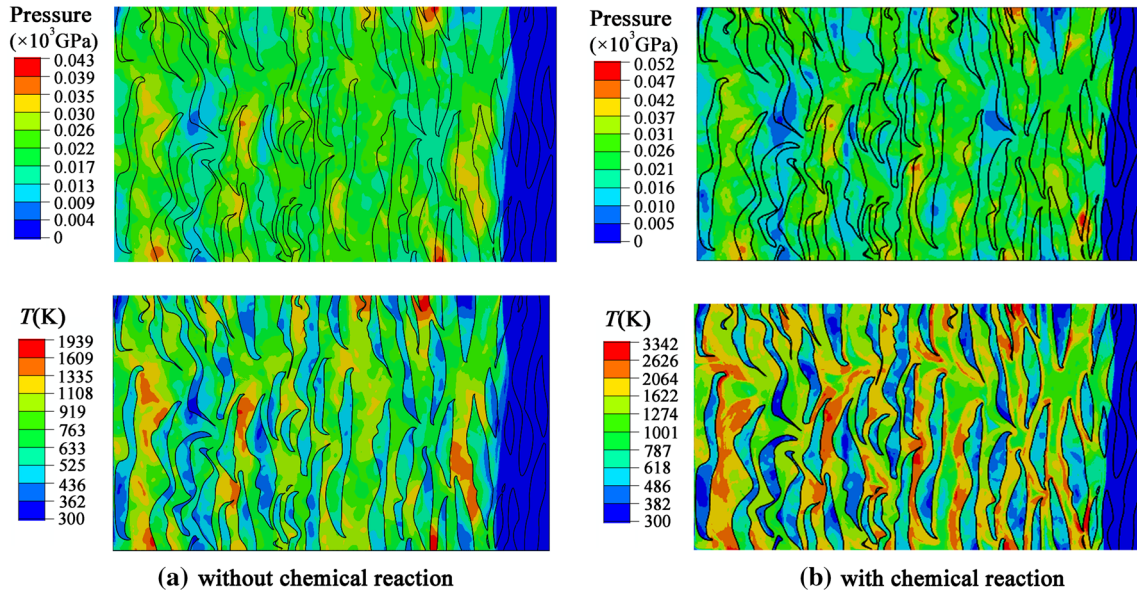


**Figure 15** The comparison of shock pressure and temperature whether considering the chemical reaction.

calculation results with chemical reaction. The above analysis indicates that the chemical reaction could increase both the shock pressure and the shock temperature in the Al/Ni composite, which would promote the chemical reaction further.

*The influence of chemical reaction on Hugoniot parameters*

The propagation speed of shock waves  $U_s$  was obtained from the simulated results by dividing the propagation distance by the corresponding duration, as shown in Fig. 16. The calculated  $U_s$  revealed a linear relationship with  $U_p$  when only considering

the mechanical response during shock compression. Once the chemical reaction was initiated, the value of  $U_s$  became higher and the  $U_s$ - $U_p$  curve deviated from the original trajectory. The corresponding images in the impact-initiated experiment [16] were marked in the figure. It revealed that the deviation of  $U_s$  increased with the particle velocities, which was strong associated with the reaction efficiency. This result indicated that the propagation speed of shock waves could be accelerated by the chemical reaction of Al/Ni composites, which was also demonstrated by other researchers[21, 22].

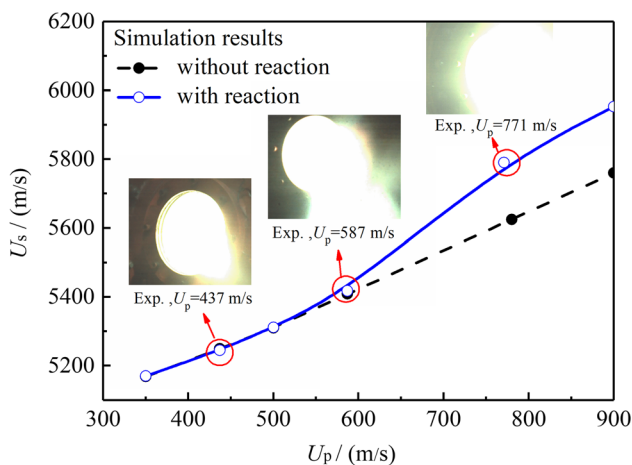


**Figure 16** The calculated  $U_s$ - $U_p$  relationship and corresponding increase rate of shock velocity in the Al/Ni composite.

**Conclusions**

A multiscale modeling method was proposed and performed on the Al/Ni multilayered composite with large particle sizes of hundreds of micrometers. The developed modeling method could obtain macroscale SICR characteristics considering microstructural effects. The connections between the dynamic response and the reaction behavior of the Al/Ni composites were deeply discussed. The following are the principal conclusions in this study:

- (1) The Arrhenius pre-exponent factor of the diffusion coefficient  $D_0$  and the pre-exponent factor for chemical reaction  $A$  were determined based on the experimental results and the one-dimension reaction-diffusion calculation

results. The further mesoscale simulation and macroscale analysis demonstrated that the two determined parameters are appropriate for the multiscale model considering unidirectional diffusion process to describe the shock reaction in Al/Ni multilayered composites with particle sizes of hundreds of micrometers.

- (2) Both the one-dimension microscopic model and the mesoscale model revealed that the mass diffusion and reaction process in the Al/Ni composites was significantly influenced by the loading conditions. Particle velocity below  $437 \text{ m s}^{-1}$  caused low shock temperature and resulted in no reaction, which could be regarded as the critical condition to initiate shock reactions in the Al/Ni multilayered composite. The increase of particle velocity and shock temperature accelerated the diffusion and reaction process.
- (3) It appears that an increase of loading period leads to a monotonic increase of the molar concentration of the reaction product, which immediately increase both the mass of the reaction product and the reaction efficiency. The reaction products continued growing even when the shock wave had propagated through the materials.
- (4) Compared with the simulation results only considering the mechanical response of the Al/Ni composite, the temperature, the shock pressure, as well as the shock velocity were found increased by the shock reaction behavior.

Generally, the multiscale modeling method give a good description on the SICR behavior of Al/Ni composites, which is an essential step to design and control the properties of this kind of composites.

## Acknowledgements

This work was funded by the National Natural Science Foundation of China (No. 12141202 and 12002170), the opening project of State Key Laboratory of Explosion Science and Technology (Beijing Institute of Technology) (KFJJ21-11M), and the Fundamental Research Funds for the Central Universities (No. 30920021108).

## References

- [1] Eakins DE, Thadhani NN (2006) Shock-induced reaction in a flake nickel+ spherical aluminum powder mixture. *J Appl Phys* 100:113521. <https://doi.org/10.1063/1.2396797>
- [2] Herbold EB, Thadhani NN, Jordan JL (2011) Observation of a minimum reaction initiation threshold in ball-milled Ni+ Al under high-rate mechanical loading. *J Appl Phys* 109:066108. <https://doi.org/10.1063/1.3549822>
- [3] Reeves RV, Mukasyan AS, Son SF (2010) Thermal and impact reaction initiation in Ni/Al heterogeneous reactive systems. *J Phys Chem C* 114:14772–14780. <https://doi.org/10.1021/jp104686z>
- [4] Wei CT, Maddox BR, Stover AK, Weihs TP, Nesterenko VF, Meyers MA (2011) Reaction in Ni–Al laminates by laser-shock compression and spalling. *Acta Mater* 59:5276–5287. <https://doi.org/10.1016/j.actamat.2011.05.004>
- [5] Kelly SC, Thadhani NN (2016) Shock compression response of highly reactive Ni + Al multilayered thin foils. *J Appl Phys* 119:095903. <https://doi.org/10.1063/1.4942931>
- [6] Hu Q, Liu R, Zhou Q et al (2022) Effects of microstructure on mechanical and energy release properties of Ni–Al energetic structural materials. *Mater Sci Eng A* 849:143332. <https://doi.org/10.1016/j.msea.2022.143332>
- [7] Xiong W, Zhang X, Tan M, Liu C, Wu X (2016) The energy release characteristics of shock-induced chemical reaction of Al/Ni composites. *J Phys Chem C* 120:24551–24559. <https://doi.org/10.1021/acs.jpcc.6b06530>
- [8] Zhang XF, Shi AS, Zhang J, Qiao L, He Y, Guan ZW (2012) Thermochemical modeling of temperature controlled shock-induced chemical reactions in multifunctional energetic structural materials under shock compression. *J Appl Phys* 111:123501. <https://doi.org/10.1063/1.4729048>
- [9] Austin RA, McDowell DL, Benson DJ (2012) Mesoscale simulation of shock wave propagation in discrete Ni/Al powder mixtures. *J Appl Phys* 111:123511. <https://doi.org/10.1063/1.4729304>
- [10] Austin RA, McDowell DL, Benson DJ (2006) Numerical simulation of shock wave propagation in spatially-resolved particle systems. *Model Simul Mater Sc* 14:537–561. <https://doi.org/10.1088/0965-0393/14/4/001>
- [11] Eakins DE, Thadhani NN (2008) Mesoscale simulation of the configuration-dependent shock-compression response of Ni+ Al powder mixtures. *Acta Mater* 56:1496–1510. <https://doi.org/10.1016/j.actamat.2007.12.009>
- [12] Eakins DE, Thadhani NN (2007) Discrete particle simulation of shock wave propagation in a binary Ni+ Al powder mixture. *J Appl Phys* 101:043508. <https://doi.org/10.1063/1.368197>
- [13] Smith GD, Bardenhagen S, Nairn JA et al (2021) Insight into the role of interfaces on mechanical properties of low-porosity

- Al/Ni compacts: comparison of experiment and simulation. *J Appl Phys* 130:105104. <https://doi.org/10.1063/5.0057074>
- [14] Smith G, Bardenhagen S, Nairn J (2020) Mesoscale modeling of Al/Ni composites. *Int J Impact Eng* 140:103537. <https://doi.org/10.1016/j.ijimpeng.2020.103537>
- [15] Smith GD, Hooper J, Bedrov D (2018) Mesoscale simulations of uniaxial compression and shock loading of low porosity granular aluminum/nickel composites. *J Appl Phys* 124:145105. <https://doi.org/10.1063/1.5042663>
- [16] Xiong W, Zhang X, Zheng L, Bao K, Chen H, Guan Z (2019) The shock-induced chemical reaction behaviour of Al/Ni composites by cold rolling and powder compaction. *J Mater Sci* 54:6651–6667. <https://doi.org/10.1007/s10853-019-03357-3>
- [17] Qiao L, Zhang XF, He Y, Shi AS, Guan ZW (2013) Mesoscale simulation on the shock compression behaviour of Al–W–Binder granular metal mixtures. *Mater Design* 47:341–349. <https://doi.org/10.1016/j.matdes.2012.12.013>
- [18] Do IP, Benson DJ (2000) Modeling shock-induced chemical reactions. *Int J Eng Sci* 1:61–69. <https://doi.org/10.1142/S1465876300000057>
- [19] Do IP, Benson DJ (2001) Micromechanical modeling of shock-induced chemical reactions in heterogeneous multi-material powder mixtures. *Int J Plasticity* 17:641–668. [https://doi.org/10.1016/S0749-6419\(00\)00065-6](https://doi.org/10.1016/S0749-6419(00)00065-6)
- [20] Qiao L, Zhang XF, He Y, Zhao XN, Guan ZW (2013) Multiscale modelling on the shock-induced chemical reactions of multifunctional energetic structural materials. *J Appl Phys* 113:173513. <https://doi.org/10.1063/1.4803712>
- [21] Lomov I, Herbold EB, Austin RA (2012) 7th Biennial Conference of the American-Physical-Society-Topical-Group on Shock Compression of Condensed Matter AIP Publishing, Chicago
- [22] Reding DJ (2010) Multiscale chemical reactions in reactive powder metal mixtures during shock compression. *J Appl Phys* 108:024905. <https://doi.org/10.1063/1.3455850>
- [23] Reding DJ, Hanagud S (2009) Chemical reactions in reactive powder metal mixtures during shock compression. *J Appl Phys* 105:024912. <https://doi.org/10.1063/1.2976313>
- [24] SivaPrasad AVS, Basu S (2015) Numerical modelling of shock-induced chemical reactions (SICR) in reactive powder mixtures using smoothed particle hydrodynamics (SPH). *Model Simul Mater Sci* 23:075005. <https://doi.org/10.1088/0965-0393/23/7/075005>
- [25] Cherukara MJ, Germann TC, Kober EM, Strachan A (2014) Shock loading of granular Ni/Al composites. Part 1: mechanics of loading. *J Phys Chem C* 118:26377–26386. <https://doi.org/10.1021/jp507795w>
- [26] Cherukara MJ, Germann TC, Kober EM, Strachan A (2016) Shock loading of granular Ni/Al composites. Part 2: shock-induced chemistry. *J Phys Chem C* 120:6804–68133. <https://doi.org/10.1021/acs.jpcc.5b11528>
- [27] Xiong Y, Xiao S, Deng H, Zhu W, Hu W (2017) Investigation of the shock-induced chemical reaction (SICR) in Ni + Al nanoparticle mixtures. *Phys Chem Chem Phys* 19:17607–17617. <https://doi.org/10.1039/c7cp03176a>
- [28] Cherukara MJ, Weihs TP, Strachan A (2015) Molecular dynamics simulations of the reaction mechanism in Ni/Al reactive intermetallics. *Acta Mater* 96:1–9. <https://doi.org/10.1016/j.actamat.2015.06.008>
- [29] Xiong Y, Li X, Xiao S et al (2019) Molecular dynamics simulations of shock loading of nearly fully dense granular Ni–Al composites. *Phys Chem Chem Phys* 21:20252–20261. <https://doi.org/10.1039/c9cp02920f>
- [30] Wei CT, Vitali E, Jiang F et al (2012) Quasi-static and dynamic response of explosively consolidated metal–aluminum powder mixtures. *Acta Mater* 60:1418–1432. <https://doi.org/10.1016/j.actamat.2011.10.027>
- [31] Dongare AM (2019) Challenges to model the role of heterogeneities on the shock response and spall failure of metallic materials at the mesoscales. *J Mater Sci* 55:3157–3166. <https://doi.org/10.1007/s10853-019-04260-7>
- [32] Lemons DS, Lund CM (1999) Thermodynamics of high temperature. Mie-Grüneisen solids *Am J Phys* 67:1105–1108. <https://doi.org/10.1119/1.19091>
- [33] Tang WH, Zhang RQ (2008) Introduction to theory and computation of equation of state. Higher Education Press, Beijing

**Publisher's Note** Springer Nature remains neutral with regard to jurisdictional claims in published maps and institutional affiliations.

Springer Nature or its licensor (e.g. a society or other partner) holds exclusive rights to this article under a publishing agreement with the author(s) or other rightsholder(s); author self-archiving of the accepted manuscript version of this article is solely governed by the terms of such publishing agreement and applicable law.